ACS APPLIED MATERIALS & INTERFACES

Research Article

www.acsami.org

Mn−Ni Content-Dependent Structures and Electrochemical Behaviors of Serial $Li_{1.2}Ni_{0.13+x}Co_{0.13}Mn_{0.54-x}O_2$ as Lithium-Ion Battery Cathodes

Chenhao Zhao, Xinxin Wang, Xinru Liu, He Zhang, and Qiang Shen*

Key Laboratory for Colloid and Interface Chemistry of Education Ministry, School of Chemistry and Chemical Engineering, Shandong University, Jinan 250100, China

ABSTRACT: In this paper, a citric acid-assisted sol−gel route has been successfully used for the nanofabrication of serial solid solutions in a chemical formula of $Li_{1.2}Ni_{0.13+x}Co_{0.13}Mn_{0.54-x}O_2$ at the x value of −0.06, −0.03, 0, 0.03, or 0.06. Powdered X-ray diffraction (XRD) results indicate that all the solid solutions possess the well-established structural characteristics for a homogeneous solid solution of Li_2MnO_3 and $LiNi_{1/3+x}Co_{1/3}Mn_{1/3-x}O_2$ components with an increasing Li_2MnO_3 content along with the decrease of x value. Scanning electron microscope (SEM) observation and elemental analyses show that these samples are composed of polyhedral nanoparticles with a chemical composition similar to that of the corresponding raw materials. Applied as lithium-ion battery cathodes, the initial Coulombic efficiency, cycling stability, and rate capability of solid solutions are determined by their chemical compositions, giving an optimal x value within the range of −0.03 and 0.03. That is, the variation of x value in the formula $Li_{1.2}Ni_{0.13+x}Co_{0.13}Mn_{0.54-x}O_2$ should exert a great influence on the electrochemical performances of these cathodes. Anyways, these suggest an effective strategy to understand the relationship between the Mn−Ni content-dependent crystal structures and electrochemical behaviors of solid solutions.

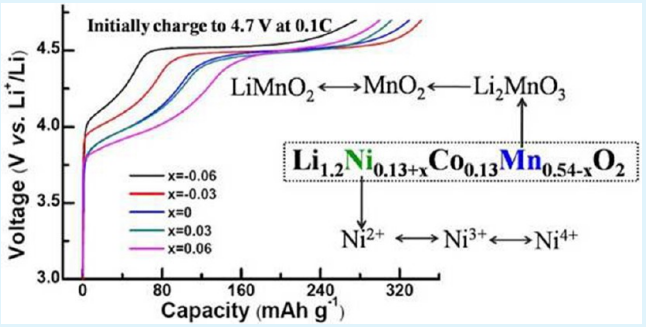

KEYWORDS: *cathode materials, solid solution, crystal structure, electrochemical behaviors, lithium-ion batteries*

1. INTRODUCTION

The exploration and development of cathode materials with high capacity, good cycling stability, and low cost are of great importance, owing to the widespread applications of lithium-ion batteries in people's daily life.[1−3] In recent years, the lithium-rich layered solid solutions in a chemical formula of $yLi_2MnO_3\cdot(1-y)LiMO_2$ ($0 < y < 1$; M = Ni, Co, Mn, Fe, Cr, $Ni_{1/2}Mn_{1/2}$, $Ni_{1/3}Co_{1/3}Mn_{1/3}$, etc.) have attracted more and more attention from specialists and have been recognized as one of the most promising candidates for the next generation of lithium-ion batteries. As for a solid solution electrode, the electrochemically "inert" constituent Li_2MnO_3 can generally stabilize the integrated crystal structure of $yLi_2MnO_3\cdot(1-y)LiMO_2$ during charge−discharge processes. However, this cannot answer for the high capacity of $yLi_2MnO_3\cdot(1-y)LiMO_2$ (>250 mAh g^{-1}). When the $yLi_2MnO_3\cdot(1-y)LiMO_2$ electrodes are charged to a potential of 4.6 V or higher, the "inert" component Li_2MnO_3 can be further activated and transformed simultaneously into another active component MnO_2. Therefore, the high discharge capacity and good cycling stability of solid solution materials can be assigned to a synergistic effect between the two components of Li_2MnO_3 and $LiMO_2$.[4−12]

As for the possible practical application of these solid solution materials as lithium-ion battery cathodes, two disadvantageous aspects still exist that need to be improved. One is a highly irreversible capacity loss in the initial cycle, which has been ascribed to the release of Li_2O from the solid solution cathode and the oxidation of $LiPF_6$-based electrolyte.[13,14] Another one is the low rate capability of solid solution cathodes, resulting from a low conductivity of the Li_2MnO_3 component and its initially transformed MnO_2.[15] Then, after the initial charge−discharge cycle the Li_2MnO_3 can be transformed into a layered structure of electrochemically active $LiMnO_2$. Then, the subsequent insertion/extraction of lithium ions into/from the homogeneous lattice structure of the solid solution can induce the Mn-dependent layer-to-spinel phase transformation. These may be the reasons why the electrode polarization increases with the continuous charge−discharge cycles, visually giving a decrease of discharge midpoint voltage estimated from the plots of voltage against discharge capacity.[13,15]

Presently, a surface modification to solid solution materials by the addition of Li-storage hosts[16−18] or a controlling synthesis of solid solutions by the modification of preparation conditions[19−21] has been mainly conducted to alleviate the above-mentioned aspects. Aside from these, a so-called optimization of chemical composition has also been recognized

Received: October 23, 2013
Accepted: January 31, 2014
Published: January 31, 2014

   dx.doi.org/10.1021/am404690z | ACS Appl. Mater. Interfaces 2014, 6, 2386−2392

Table 1. Chemical Compositions of $Li_{1.2}Ni_{0.13+x}Co_{0.13}Mn_{0.54-x}O_2$ Measured by the ICP/AES Method

	atomic ratio of ICP				
x value	Li	Ni	Co	Mn	deduced formula
−0.06	1.358	0.0736	0.1523	0.6551	$Li_{1.244}Ni_{0.067}Co_{0.139}Mn_{0.600}O_2$
−0.03	1.363	0.1106	0.1549	0.6256	$Li_{1.241}Ni_{0.100}Co_{0.141}Mn_{0.570}O_2$
0.00	1.309	0.1433	0.1527	0.5867	$Li_{1.205}Ni_{0.132}Co_{0.140}Mn_{0.540}O_2$
0.03	1.312	0.1828	0.1533	0.5626	$Li_{1.190}Ni_{0.166}Co_{0.139}Mn_{0.510}O_2$
0.06	1.333	0.2170	0.1540	0.5215	$Li_{1.227}Ni_{0.200}Co_{0.142}Mn_{0.480}O_2$

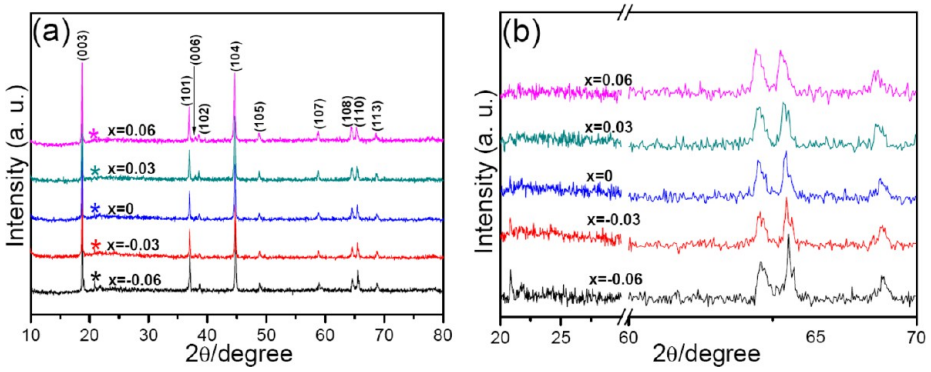

Figure 1. (a) Overall and (b) close-up XRD patterns of powdered $Li_{1.2}Ni_{0.13+x}Co_{0.13}Mn_{0.54-x}O_2$ samples obtained at the x value of −0.06, −0.03, 0, 0.03, and 0.06. In panel (a), the diffraction peaks marked with asterisks are indicative of superlattice ordering.

as an effective route to improve the electrochemical performance of solid solutions. For example, the variation of elemental content for the formulas of $Li[Li_xNi_{0.34-x}Mn_{0.47}Co_{0.19}]O_2$,[22] $Li_{1+x}Mn_{0.5+0.5x}Ni_{0.5-0.5x}O_2$,[23] $Li_{1+n}[Ni_mCo_mMn_{1-2m}]O_2$,[24] and $yLi_2MnO_3\cdot(1-y)LiNi_{1/3}Co_{1/3}Mn_{1/3}O_2$[25] could exert a great influence on the electrochemical properties of corresponding electrodes. Among all the solid solutions, $Li_{1.2}Ni_{0.13}Co_{0.13}Mn_{0.54}O_2$ (i.e., $0.5Li_2MnO_3\cdot0.5LiNi_{1/3}Co_{1/3}Mn_{1/3}O_2$) has been proved as one of the most promising cathode materials due to its high discharge capacity, moderate cycling performance, and good rate capability.[26−28]

In some sense, a minor change of chemical composition in the formula $Li_{1.2}Ni_{0.13}Co_{0.13}Mn_{0.54}O_2$ may help us to understand the structure−function relationship for a series of lithium-rich layered solid solutions and to choose the best one with an appropriate chemical composition for practical purposes. In our previous work, a study of the influence of Co content on the electrochemical behaviors of serial $Li_{1.2}Ni_{0.13+x}Co_{0.13-2x}Mn_{0.54+x}O_2$ had been conducted, giving an optimal x value within the range of 0.07−0.13.[28] Also, considering the nonnegligible contributions of Mn−Ni elements to the structural and electrochemical properties of $Li_{1.2}Ni_{0.13}Co_{0.13}Mn_{0.54}O_2$,[16−30] herein a simple citric acid-assisted sol−gel method was used to prepare another serial solid solution of $Li_{1.2}Ni_{0.13+x}Co_{0.13}Mn_{0.54-x}O_2$ (x = −0.06, −0.03, 0, 0.03, or 0.06). Thus, the main subjects of this paper deal with Mn−Ni content-dependent crystal structures and electrochemical behaviors of the as-obtained samples as lithium-ion battery cathodes, discussed in detail in the text.

2. EXPERIMENTAL SECTION

2.1. Synthesis of $Li_{1.2}Ni_{0.13+x}Co_{0.13}Mn_{0.54-x}O_2$. All the chemical reagents are of A.R. grade and were used without further purification. $Li_{1.2}Ni_{0.13+x}Co_{0.13}Mn_{0.54-x}O_2$ (x = −0.06, −0.03, 0, 0.03, or 0.06) was prepared by a simple citric acid-assisted sol−gel route, described as follows. Taking the synthesis procedure of $Li_{1.2}Ni_{0.13}Co_{0.13}Mn_{0.54}O_2$ as an example, 1.176 g of $Mn(AC)_2\cdot4H_2O$, 0.2872 g of $Ni(AC)_2\cdot4H_2O$, 0.2876 g of $Co(AC)_2\cdot4H_2O$, and 1.868 g of citric acid were dissolved into 15.0 mL of ultrapure water (18.2 MΩ.cm) at first. Then, after the addition of 0.4562 g of $LiOH\cdot H_2O$ under stirring, ammonia $NH_3\cdot H_2O$ (25−28 wt %) was dropwise added to adjust the resulting pH at a value of 8.0−9.0. Then, after a mild heat-treatment at 80 °C for the partial condensation, the resulting purple gels were in sequence dried at 140 °C for 4 h, decomposed at 450 °C for 4 h, ground uniformly, calcined at 850 °C for 12 h, and cooled naturally to room temperature. It should be pointed out that at an x value of −0.06, −0.03, 0, 0.03, or 0.06 the Ni:Co:Mn atomic ratio in the formula $Li_{1.2}Ni_{0.13+x}Co_{0.13}Mn_{0.54-x}O_2$ was estimated according to that of the corresponding raw materials.

2.2. Crystal Characterization. The chemical compositions of as-prepared samples were determined using an inductively coupled plasma/atomic emission spectrometer (ICP/AES). X-ray diffraction (XRD) patterns were collected on a Rigaku D/max-2400 powder X-ray diffractometer with Cu Kα radiation and at a rate of 0.04° step/s. Scanning electron microscopy (SEM) (JEOL JSM-7600F, 15 kV) and corresponding energy dispersive X-ray spectrometry (EDX) were conducted to characterize the morphologies, sizes, and chemical compositions of $Li_{1.2}Ni_{0.13+x}Co_{0.13}Mn_{0.54-x}O_2$ samples.

2.3. Electrochemical Characterization. After the mixing of a $Li_{1.2}Ni_{0.13+x}Co_{0.13}Mn_{0.54-x}O_2$, acetylene black, and poly(vinyl difluoride) (PVDF) at a weight ratio of 80:10:10, the resulting mixture was slurried with N-methyl-2-pyrrolidone and then pasted onto an aluminum foil and dried at 80 °C for 5 h. Finally, the aluminum foil was cut into discs with a diameter of 12 mm, and the working electrode possessed a loading density of 2.6 ± 0.4 mg cm^{-2}. Glass fiber (Whatman) and commercial LBC 305-01 $LiPF_6$ solution (Shenzhen) were used as the separator and electrolyte, respectively. The CR 2032 coin cells of $Li_{1.2}Ni_{0.13+x}Co_{0.13}Mn_{0.54-x}O_2$/Li were assembled in an argon-filled glovebox. The galvanostatic cycling tests were conducted on a Land CT2001A battery system at room temperature. Alternating-current electrochemical impedance spectra (AC EIS) were collected on a workstation (Materials Mates 510, Italia) at frequencies from 0.1 MHz to 0.01 Hz.

3. RESULTS AND DISCUSSION

3.1. Nonelectrochemical Measurements of Serial $Li_{1.2}Ni_{0.13+x}Co_{0.13}Mn_{0.54-x}O_2$. The chemical compositions of

dx.doi.org/10.1021/am404690z | ACS Appl. Mater. Interfaces 2014, 6, 2386−2392

serial $Li_{1.2}Ni_{0.13+x}Co_{0.13}Mn_{0.54-x}O_2$ are measured by the ICP/AES method, and the obtained results are listed in Table 1. For each x value, the Ni:Co:Mn atomic ratio is almost the same as that of $(0.13 + x):0.13:(0.54 - x)$, and the elemental content of lithium is close to the stoichiometric value of 1.20 (Table 1). This means that the as-prepared solid solution series can be approximately described as $Li_{1.2}Ni_{0.13+x}Co_{0.13}Mn_{0.54-x}O_2$ according to that of the corresponding raw materials.

XRD patterns of serial $Li_{1.2}Ni_{0.13+x}Co_{0.13}Mn_{0.54-x}O_2$ at different x values are shown in Figure 1. In Figure 1a, the indexed diffraction peaks coincide well with the standard data for the hexagonal structure of components $LiMO_2$ (M = $Li_{1/3}Mn_{2/3}$ and/or $Ni_{1/3}Co_{1/3}Mn_{1/3}$), which is the same as those of crystalline α-$NaFeO_2$. Also, the asterisk-marked weak diffraction peaks in the 2θ range of 20−25° belong to the superlattice ordering characteristics for the periodic occupation of Li^+ ions in the transition metal layers of a $LiMO_2$ lattice unit, proving the coexistence of the component Li_2MnO_3 (also referred to as $Li(Li_{1/3}Mn_{2/3})O_2$ formula) in the homogeneous crystal phases of the solid solution materials.[10−17] Especially, a section of Figure 1a from 20° to 30° and 60° to 70° is magnified and shown as Figure 1b, and the supperlattice ordering diffraction peaks located nearby 21° gradually weaken with the increase of x values, indicating that the content of the Li_2MnO_3 component is reduced in these chemical formulas.

Generally speaking, the lattice parameters of a hexagonal structure ($a = b \neq c$, $\alpha = \beta = 90°$, $\gamma = 120^o$) are determined by the chemical composition and atomic arrangement of the lithium-rich layered materials. Resembling the XRD peak intensity ratio of (003) to (104) ($I_{(003)}/I_{(104)}$), the lattice parameter ratio of c to a (c/a) can also be used to measure the structural ordering and cation mixing, and the higher value of c/a (or, $I_{(003)}/I_{(104)}$) means better layered structural ordering and lower cation mixing.[29,31] From the XRD data and space group $R\bar{3}m$ of serial $Li_{1.2}Ni_{0.13+x}Co_{0.13}Mn_{0.54-x}O_2$, the lattice parameters of a and c and the ratios of c/a, $I_{(003)}/I_{(104)}$, and $I_{(110)}/I_{(108)}$ are estimated and revealed in Table 2. For each solid solution,

Table 2. Lattice Parameters a and c and Ratios c/a, $I_{(003)}/I_{(104)}$, and $I_{(110)}/I_{(108)}$ for Different $Li_{1.2}Ni_{0.13+x}Co_{0.13}Mn_{0.54-x}O_2$ Samples Calculated from the Refined XRD Data and Space Group $R\bar{3}m$

x value	a (Å)	c (Å)	c/a	$I_{(003)}/I_{(104)}$	$I_{(110)}/I_{(108)}$
−0.06	2.843	14.200	4.995	1.32	1.85
−0.03	2.847	14.221	4.995	1.33	1.62
0	2.849	14.228	4.994	1.11	1.22
0.03	2.853	14.219	4.984	1.22	1.15
0.06	2.854	14.234	4.987	1.06	1.07

the lattice parameter of a or c is about 2.85 or 14.22 Å, which is close to that of single-crystalline $LiNi_{1/3}Co_{1/3}Mn_{1/3}O_2$.[29,31] Also, the c/a, $I_{(003)}/I_{(104)}$, and $I_{(110)}/I_{(108)}$ ratios decrease with increasing Ni content (i.e., the increasing x value) as shown in Table 2. These are consistent with Liu's results that, based on the approximate ion radii of Ni^{2+} (~0.069 nm) and Li^+ (~0.076 nm) ions, the solid solution with a high Ni content will have a high cation mixing in the lattice structure.[30−32]

Figure 2 shows the SEM images and corresponding EDX spectra of $Li_{1.2}Ni_{0.13+x}Co_{0.13}Mn_{0.54-x}O_2$ samples. All the samples are composed of polyhedral nanoparticles, and parts of them visually possess sharp edges and smooth facets (Figure 2a, c, e, g, and i), indicating that these solid solutions are well crystallized. At the x value of −0.06, −0.03, 0, 0.03, or 0.06, the estimated average particle size is 520.6 ± 151.1, 315.0 ± 52.5, 195.0 ± 44.4, 216.1 ± 56.7, or 221.4 ± 50.4 nm. This indicates that the chemical composition of a solid solution may play an important role in its nucleation and crystal growth.[28,33] According to the EDX spectra of serial $Li_{1.2}Ni_{0.13+x}Co_{0.13}Mn_{0.54-x}O_2$ shown in Figure 2b, d, f, h, and j, the obtained atomic ratios can hardly be indicative of the corresponding chemical compositions but can reflect the chemical uniformity of polyhedral nanoparticles to a great extent.

3.2. Electrochemical Measurements of Serial $Li_{1.2}Ni_{0.13+x}Co_{0.13}Mn_{0.54-x}O_2$.

As lithium-ion battery cathodes, one of the most attractive advantages of serial $Li_{1.2}Ni_{0.13+x}Co_{0.13}Mn_{0.54-x}O_2$ (also defined as an ideal formula of $0.5Li_2MnO_3{\cdot}0.5LiNi_{1/3+x}Co_{1/3}Mn_{1/3-x}O_2$) is the relatively high reversible capacity between 200 and 300 mAh g^{-1}. However, the initial activation of the Li_2MnO_3 component will lead to a highly irreversible capacity loss, giving a low Coulombic efficiency. Figure 3 and Table 3 comparatively present the initial charge−discharge data of $Li_{1.2}Ni_{0.13+x}Co_{0.13}Mn_{0.54-x}O_2$ series collected within the electrochemical window of 2.0 and 4.7 V at a low current density of 20 mA g^{-1}. As for the initial charge curves of serial $Li_{1.2}Ni_{0.13+x}Co_{0.13}Mn_{0.54-x}O_2$ shown in Figure 3, the charging plateau of ~4.5 V is more obvious at a lower x value (or a higher Mn content).

When the x value is −0.06, −0.03, 0, 0.03, or 0.06, the working electrode gives a specific discharge capacity of 169.4, 242.1, 267.6, 240.4, or 225.2 mAh g^{-1} with a Coulombic efficiency of 61.3%, 70.7%, 81.1%, 77.1%, or 73.1% (Figure 3, Table 3). That is, a slight change of x value to the optimal $Li_{1.2}Ni_{0.13+x}Co_{0.13}Mn_{0.54-x}O_2$ ($x = 0$) is unfavorable, leading to the decrease of both initial discharge capacity and the corresponding Coulombic efficiency. This is similar to Thackeray and Yang's conclusion that, at the equal stoichiometric ratio of Li_2MnO_3 to $LiNi_{1/3}Co_{1/3}Mn_{1/3}O_2$ (i.e., $y = 0.5$), the discharge capacity of $yLi_2MnO_3{\cdot}(1 - y)LiMO_2$ is higher than those of the others (e.g., $y = 0.4$ or 0.6).[34,35]

To further understand the influence of x value on the reversible intercalation−extraction of lithium ions, the initial charge and discharge profiles of serial $Li_{1.2}Ni_{0.13+x}Co_{0.13}Mn_{0.54-x}O_2$ electrodes were transformed into differential capacity (dQ/dV) curves, are shown in Figure 4a and b, respectively. In Figure 4a, each anodic peak at ~4.0 V can be ascribed to the deintercalation of Li^+ ions from layered lattice accompanied by the oxidation of Ni^{2+} ions within the $LiNi_{1/3+x}Co_{1/3}Mn_{1/3-x}O_2$ phase, and the sharp peaks at 4.4−4.6 V correspond to both the loss of Li_2O from the Li_2MnO_3 phase to form layered MnO_2 and the oxidation of Co^{3+} ions within the active component.[33,34] Also, it can be clearly seen that, with the increase of x value, the ~4.0 V anodic peak gradually shifts to the lower voltage positions as indicated by the dashed line, indicating the material with higher x value has a lower internal resistance and better electron conductivity (Figure 4a). It is well-known that, for the serial solid solutions of $Li_{1.2}Ni_{0.13+x}Co_{0.13}Mn_{0.54-x}O_2$, the component Li_2MnO_3 generally possesses much lower conductivity than the $LiNi_{1/3+x}Co_{1/3}Mn_{1/3-x}O_2$ component.[15] According to the XRD results shown in Figure 1, the solid solution with a low x value (i.e., with a low percentage of component Li_2MnO_3) should have a low electron conductivity when applied as a lithium-ion battery cathode.

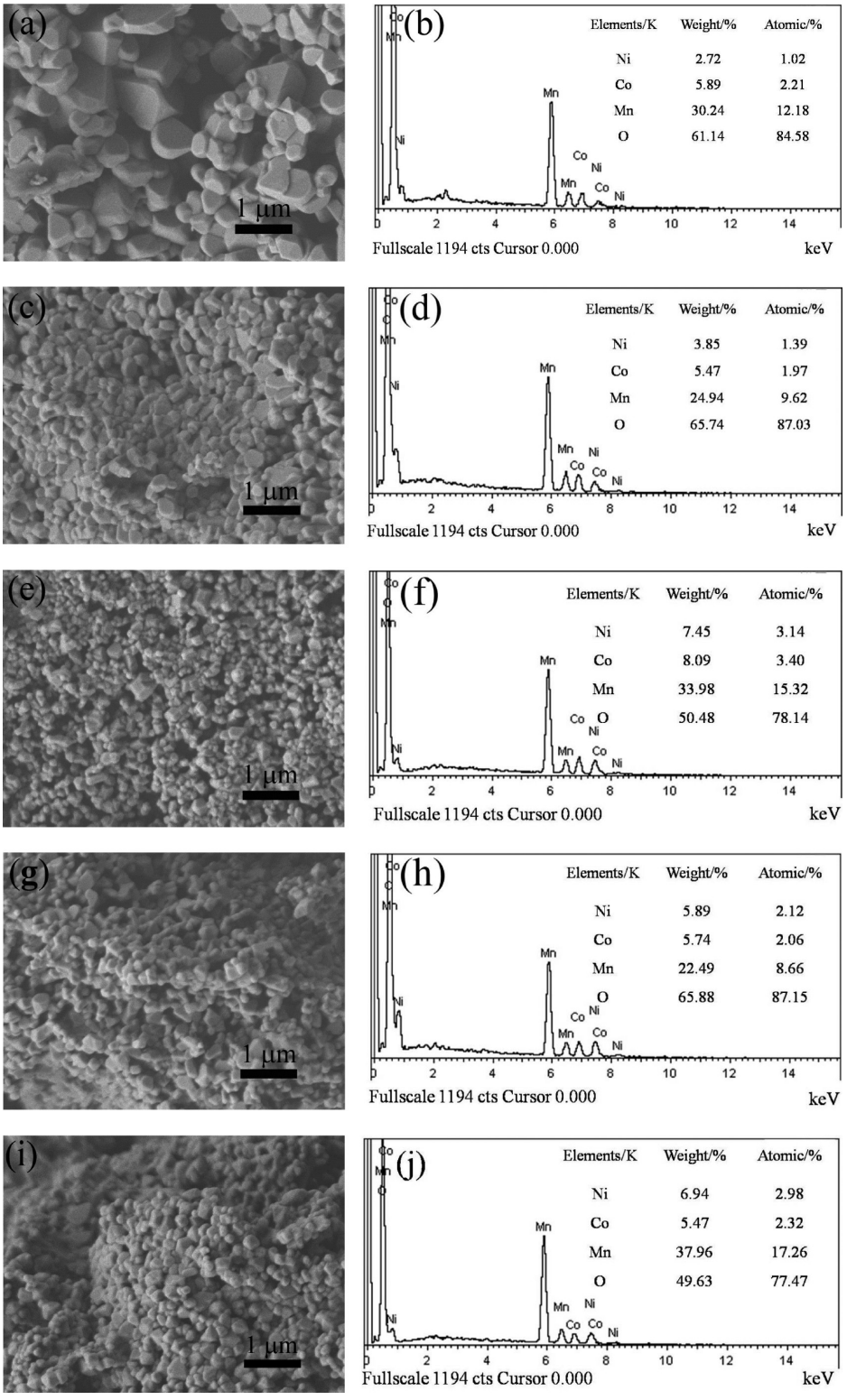

Figure 2. SEM images and corresponding EDX spectra of serial $Li_{1.2}Ni_{0.13+x}Co_{0.13}Mn_{0.54-x}O_2$ at the x values of (a, b) −0.06, (c, d) −0.03, (e, f) 0, (g, h) 0.03, or (i, j) 0.06.

In Figure 4b, a wide cathodic peak nearby 3.6 V may be attributed to the reduction of Ni^{4+} to Ni^{2+} accompanied with the intercalation of Li^+ ions, while the other peak at 2.5 V could correspond to the reduction of MnO_2 for the in situ generation of active $LiMnO_2$. In the first charge−discharge cycle, the irreversible transformation of $Li_2MnO_3 \rightarrow MnO_2 \rightarrow LiMnO_2$ may account for the high-capacity feature of these solid solutions at each x value. Also in Figure 4b, the cathodic peak at 2.5 V disappears at the high x values of 0.03 and 0.06, wherein the electrochemical signal for the reduction of MnO_2 may be completely integrated into that of the ∼3.6 V peak.[27,28] As shown in Figure 4b, the peak potential marked by the inclined dashed line decreases with the increasing x value, which corresponds to the change of discharge midpoint voltage shown

dx.doi.org/10.1021/am404690z | ACS Appl. Mater. Interfaces 2014, 6, 2386−2392

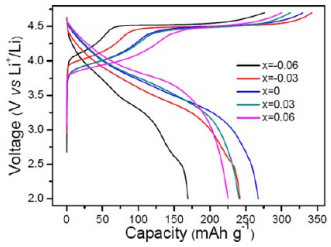

Figure 3. Initial charge−discharge curves of serial $Li_{1.2}Ni_{0.13+x}Co_{0.13}Mn_{0.54-x}O_2$ electrodes recorded at 20 mA g^{-1} between 2.0 and 4.7 V.

Table 3. Initial Charge Capacity, Discharge Capacity, Coulumbic Efficiency, and Discharge Midpoint Voltage of $Li_{1.2}Ni_{0.13+x}Co_{0.13}Mn_{0.54-x}O_2$ Electrodes Obtained at 20 mA g^{-1} between 2.0 and 4.7 V

x value	charge capacity (mAh g^{-1})	discharge capacity (mAh g^{-1})	Coulombic efficiency (%)	discharge midpoint voltage (V)
−0.06	276.1	169.4	61.3	3.40
−0.03	342.2	242.1	70.7	3.50
0	329.9	267.6	81.1	3.57
0.03	311.9	240.4	77.1	3.67
0.06	300.2	225.2	75.0	3.79

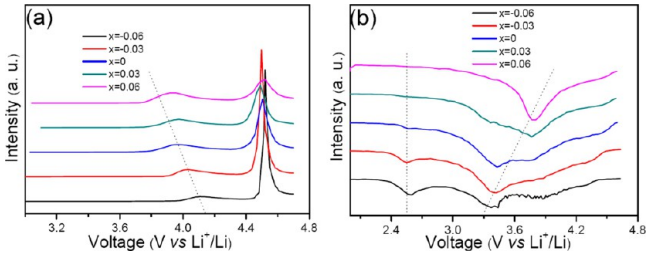

Figure 4. Differential capacity (dQ/dV) profiles of serial $Li_{1.2}Ni_{0.13+x}Co_{0.13}Mn_{0.54-x}O_2$ electrodes: (a) the initial anodic processes and (b) the initial cathodic processes.

in Table 3. Theoretically, the electrochemical reduction potential of $Ni^{4+} \rightarrow Ni^{2+}$ (3.8−4.4 V) is higher than that of $MnO_2 \rightarrow LiMnO_2$ (~3.0 V), thus the solid solution $Li_{1.2}Ni_{0.13+x}Co_{0.13}Mn_{0.54-x}O_2$ with a relatively high Ni content should have a high discharge midpoint voltage.

Owing to the initial activation of Li_2MnO_3 within 2.0 and 4.7 V, it is better to study the discharge capacity-dependent (or midpoint voltage-dependent) durability of serial $Li_{1.2}Ni_{0.13+x}Co_{0.13}Mn_{0.54-x}O_2$ after an initially low-rate (e.g., 20 mA g^{-1}) charge−discharge cycling test. As shown in Figure 5a,

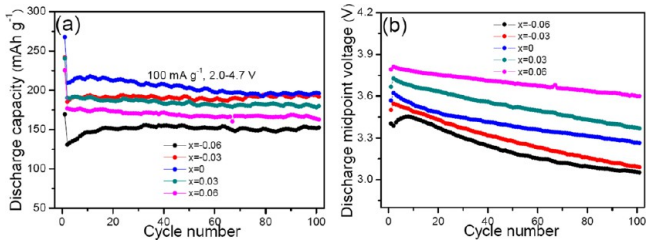

Figure 5. Plots of (a) discharge capacity and (b) discharge midpoint voltage against cycle number for serial $Li_{1.2}Ni_{0.13+x}Co_{0.13}Mn_{0.54-x}O_2$ electrodes.

at a current density of 100 mA g^{-1} the second specific discharge capacities of them are 130.7, 185.1, 209.3, 190.2, and 176.6 mAh g^{-1} at the x value of −0.06, −0.03, 0, 0.03, and 0.06, respectively. Over 100 cycles, the residual values are 152.8, 191.8, 195.9, 179.8, and 162.8 mAh g^{-1}, accordingly giving a retention ratio of 116.9%, 103.6%, 93.6%, 94.5%, and 92.2%. These mean that the increase of x value can awake the decay of the cycling stability of $Li_{1.2}Ni_{0.13+x}Co_{0.13}Mn_{0.54-x}O_2$ cathodes. Furthermore, the comparative durabilities show that the low x value sample (i.e., x = −0.06 or −0.03) has an increased discharge capacity upon cycling (Figure 5a), which might be attributed to an increase of active surface area and/or the continuous activation of the Li_2MnO_3 component as reported by Oh et al.[36]

As shown in Figure 5b, at each x value the variation of discharge midpoint voltage greatly differs from that of discharge capacity shown in Figure 5a. That is, for the serial $Li_{1.2}Ni_{0.13+x}Co_{0.13}Mn_{0.54-x}O_2$, all the discharge midpoint voltages sharply decrease along with the continuous charge−discharge cycle. By comparison, a solid solution with the higher x value can keep more stable discharge midpoint voltage upon cycling (Figure 5b), which can be simply assigned to the higher Ni content (or the lower Mn content) of the electrode discussed below.

Upon the continuous cycling, the second, 26th, 51st, and 101st charge−discharge profiles and corresponding dQ/dV profiles of serial $Li_{1.2}Ni_{0.13+x}Co_{0.13}Mn_{0.54-x}O_2$ electrodes are revealed in Figure 6. All the solid solutions experience a gradual decay of discharge midpoint voltage from the second to the 101st cycle (Figure 6a, c, e, g, and i), and this is due to a combined potential shift of the layered Co^{4+}/Co^{3+}, Ni^{4+}/Ni^{2+}, and spinel Mn^{4+}/Mn^{3+} peaks along with the galvanostatic cycles (Figure 6b, d, f, h, and j). As the cycle number increases, the cathodic peak of the layered Ni^{4+}/Ni^{2+} nearby 3.8 V weakens gradually, and the cathodic peak of the spinel Mn^{4+}/Mn^{3+} nearby 3.0 V increases step by step. This means that, for all the solid solutions, parts of the layered structure can be gradually transformed into the spinel structure in crystallography.[13−16] Especially, the formation of spinel Li−Mn−O can be effectively suppressed by the decrease of Mn content or the increase of Ni content (i.e., the increase of x value).

The rate capabilities of various $Li_{1.2}Ni_{0.13+x}Co_{0.13}Mn_{0.54-x}O_2$ electrodes are revealed in Figure 7. It is shown that, after the initial activation of Li_2MnO_3 at the first cycle, the specific discharge capacity of each sample gradually decreases with the increasing current rate from 20 to 1000 mA g^{-1}. The 22nd specific discharge capacity is 76.9 (x = −0.06), 135.0 (x = −0.03), 164.0 (x = 0), 150.7 (x = 0.03), or 145.3 (x = 0.06) mAh g^{-1} at 400 mA g^{-1}, and the 32nd reversible capacity at 1000 mA g^{-1} still keeps at a value of 52.5 (x = −0.06), 102.5 (x = −0.03), 127.8 (x = 0), 127.8 (x = 0.03), or 120.0 (x = 0.06) mAh g^{-1}. Importantly, as shown in Figure 7, when the current density goes back to 20 mA g^{-1}, the 52nd cycle discharge capacity returns to a high value of 202.6 (x = −0.06), 239.4 (x = −0.03), 256.1 (x = 0), 238.7 (x = 0.03), or 220.8 (x = 0.06). The discharge capacity ratio of the 32nd to 52nd cycle is 25.9% (x = −0.06), 42.8% (x = −0.03), 49.9% (x = 0), 53.5% (x = 0.03), or 54.3% (x = 0.06), indicating that the rate capability of serial $Li_{1.2}Ni_{0.13+x}Co_{0.13}Mn_{0.54-x}O_2$ could be improved by the increasing x value. On the basis of the considerable discharge capacities of the series at 1000 mA g^{-1}, the one with a high x value (i.e., 0, 0.03, or 0.06) may be suitable for the high-rate intercalation/extraction processes of lithium ions.

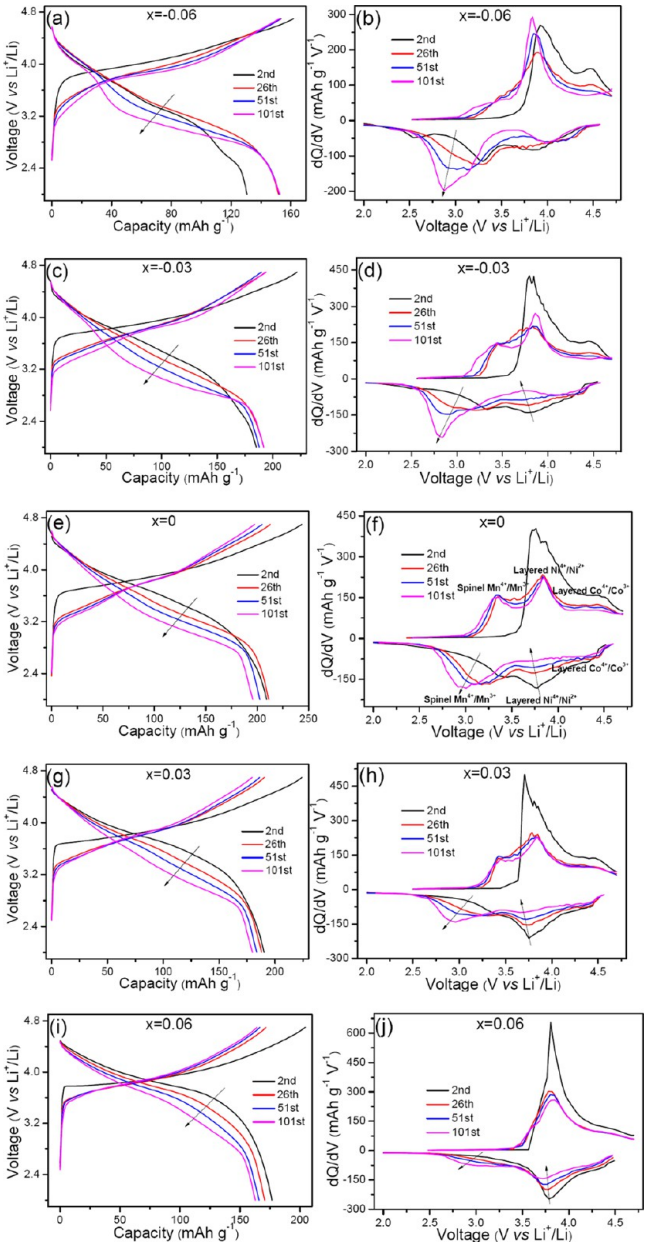

Figure 6. Second, 26th, 51st, and 101st charge−discharge profiles and corresponding dQ/dV profiles of serial $Li_{1.2}Ni_{0.13+x}Co_{0.13}Mn_{0.54-x}O_2$ electrodes obtained at the x value of (a, b) −0.06, (c, d) −0.03, (e, f) 0, (g, h) 0.03, and (i, j) 0.06.

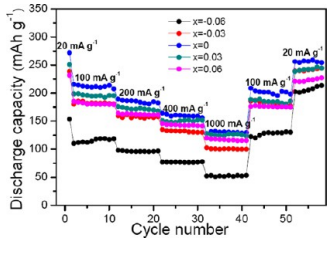

Figure 7. High-rate cycling stability of serial $Li_{1.2}Ni_{0.13+x}Co_{0.13}Mn_{0.54-x}O_2$ electrodes.

AC EIS measurements of serial $Li_{1.2}Ni_{0.13+x}Co_{0.13}Mn_{0.54-x}O_2$ electrodes after the initial two charge−discharge cycles are carried out for a comparison purpose. As shown in Figure 8, all

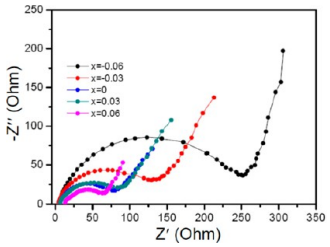

Figure 8. EIS results of serial $Li_{1.2}Ni_{0.13+x}Co_{0.13}Mn_{0.54-x}O_2$ electrodes recorded after the initial two charge−discharge cycles.

the Nyquist plots give a high-frequency semicircle and a low-frequency slope line, corresponding to an electrolyte−electrode interfacial resistance of charge transfer (R_{ct}) and a Warburg impedance of lithium diffusion within the electrode, respectively. When the x value is −0.06, −0.03, 0, 0.03, or 0.06, the working electrode possesses an approximate R_{ct} value of 257, 151, 89, 92, or 60 Ω. That is, for the serial $Li_{1.2}Ni_{0.13+x}Co_{0.13}Mn_{0.54-x}O_2$ cathodes, their charge-transfer resistances decrease with the increasing x value (i.e., the increasing Ni content or the decreasing Mn content). This is the reason why the solid solution with a relatively low Mn content (e.g., x = 0.03 or 0.06) has a relatively high rate capability as the comparative results show in Figure 7.

4. CONCLUSION

Serial solid solutions of $Li_{1.2}Ni_{0.13+x}Co_{0.13}Mn_{0.54-x}O_2$ (x = −0.06, −0.03, 0, 0.03, 0.06) have been successfully prepared by a citric acid-assisted sol−gel route. Varying with the x value (i.e., Ni and/or Mn content), all the homogeneous solid solutions of Li_2MnO_3 and $LiNi_{1/3+x}Co_{1/3}Mn_{1/3-x}O_2$ are composed of polyhedral nanoparticles with clear edges and smooth facets. By comparison, the solid solution with a high Ni content (or a high x value) has a low structural ordering and a high cation mixing in crystallography. Applied as lithium-ion battery cathodes within 2.0 and 4.7 V, these solid solutions exhibit Mn−Ni content-dependent electrochemical properties, giving an optimal x value in the range of −0.03 and 0.03. Comparatively, the $x \sim 0$ sample gives the lower initial capacity loss (discharge capacity ~267.6 mAh g^{-1}, Coulombic efficiency ~81.1%, 20 mA g^{-1}); the $x \sim -0.03$ sample acquires the better cycling stability (the 100th reversible capacity ~194.1 mAh g^{-1}, 100 mA g^{-1}); and the $x \sim 0.03$ sample possesses the higher rate capability (specific capacity ~127.8 mAh g^{-1}, 1000 mA g^{-1}). Anyway, an optimal chemical composition of the serial solid solutions should be considered for practical purposes, deserving to be conducted continuously.

AUTHOR INFORMATION

Corresponding Author

*Tel.: +86-531-88361387. Fax: +86-531-88364464. E-mail: qshen@sdu.edu.cn.

Notes

The authors declare no competing financial interest.

ACKNOWLEDGMENTS

The authors thank the financial support from the National Basic Research Program of China (2011CB935900) and from Shandong Province (ZR2012BM001).

REFERENCES

(1) Ellis, B. L.; Lee, K. T.; Nazar, L. F. *Chem. Mater.* **2010**, *22*, 691−714.
(2) Goodenough, J. B.; Kim, Y. S. *Chem. Mater.* **2010**, *22*, 587−603.
(3) He, P.; Yu, H. J.; Li, D.; Zhou, H. S. *J. Mater. Chem.* **2012**, *22*, 3680−3695.
(4) Thackeray, M. M.; Johnson, C. S.; Vaughey, J. T.; Li, N.; Hackney, S. A. *J. Mater. Chem.* **2005**, *15*, 2257−2267.
(5) Thackeray, M. M.; Kang, S. H.; Johnson, C. S.; Vaughey, J. T.; Benedek, R.; Hackney, S. A. *J. Mater. Chem.* **2007**, *17*, 3112−3125.
(6) Min, J. W.; Yim, C. J.; Im, W. B. *ACS Appl. Mater. Interfaces* **2013**, *5*, 7765−7769.
(7) Zheng, J. M.; Wu, X. B.; Yang, Y. *Electrochim. Acta* **2011**, *56*, 3071−3078.
(8) Jiang, K. C.; Wu, X. L.; Yin, Y. X.; Lee, J. S.; Kim, J.; Guo, Y. G. *ACS Appl. Mater. Interfaces* **2012**, *4*, 4858−4863.
(9) Wu, Y.; Manthiram, A. *J. Power Sources* **2008**, *183*, 749−754.
(10) Wang, J.; Yao, X. Y.; Zhou, X. F.; Liu, Z. P. *J. Mater. Chem.* **2011**, *21*, 2544−2549.
(11) Yu, H. J.; Ishikawa, R.; So, Y. G.; Shibata, N.; Kudo, T.; Zhou, H. S.; Ikuhara, Y. *Angew. Chem., Int. Ed.* **2013**, *52*, 5969−5973.
(12) Yu, H. J.; Zhou, H. S. *J. Phys. Chem. Lett.* **2013**, *4*, 1268−1280.
(13) Liu, J. L.; Chen, L.; Hou, M. Y.; Wang, F.; Che, R. C.; Xia, Y. Y. *J. Mater. Chem.* **2012**, *22*, 25380−25387.
(14) Kobayashi, H.; Takenaka, Y.; Arachi, Y.; Nitani, H.; Okumura, Y. *Solid State Ionics* **2012**, *225*, 580−584.
(15) Zhao, T. L.; Chen, S.; Li, L.; Zhang, X. F.; Wu, F.; Amine, K. *J. Power Sources* **2013**, *228*, 206−213.
(16) Gao, J.; Kim, J.; Manthiram, A. *Electrochem. Commun.* **2009**, *11*, 84−86.
(17) Wang, Z. Y.; Liu, E. Z.; He, C. N.; Li, J. J.; Zhang, N. Q. *J. Power Sources* **2013**, *236*, 25−32.
(18) Liu, J.; Manthiram, A. *J. Mater. Chem.* **2010**, *20*, 3961−3967.
(19) Xia, X. D.; Li, X. Q.; Li, W. S. *J. Power Sources* **2013**, *230*, 89−95.
(20) Lin, J.; Mu, D. B.; Lin, Y.; Wu, B. R.; Wu, F. *J. Power Sources* **2013**, *230*, 76−80.
(21) Shi, S. J.; Tu, J. P.; Tang, Y. Y.; Wang, X. L. *J. Power Sources* **2013**, *221*, 300−307.
(22) Zhang, X. H.; Yu, C.; Huang, X. D.; Zheng, J.; Guan, X. F.; Luo, D.; Li, L. P. *Electrochim. Acta* **2012**, *81*, 233−238.
(23) Yu, C.; Li, G. S.; Guang, X. F.; Zheng, J.; Li, L. P. *Electrochim. Acta* **2012**, *61*, 216−228.
(24) Li, F.; Zhao, S. X.; Wang, K. Z.; Li, B. H.; Nan, C. W. *Electrochim. Acta* **2013**, *97*, 17−22.
(25) Toprakci, O.; Toprakci, H.; Li, Y.; Ji, L. W.; Xue, L. G.; Lee, H.; Zhang, S.; Zhang, X. W. *J. Power Sources* **2013**, *241*, 522−528.
(26) Kang, S. H.; Kempgens, P.; Greenbaum, S.; Kropf, A. J.; Amine, K.; Thackeray, M. M. *J. Mater. Chem.* **2007**, *17*, 2069−2077.
(27) Liu, F. L.; Zhang, S.; Deng, C.; Wu, Q.; Sun, S. H. *J. Electrochem. Soc.* **2012**, *159*, A1591−A1597.
(28) Zhao, C. H.; Kang, W. P.; Liu, R.; Shen, Q. *RSC Adv.* **2013**, *2*, 2362−2368.
(29) Cho, T. H.; Shiosaki, Y.; Noguchi, H. *J. Power Sources* **2006**, *159*, 1322−1327.
(30) Yu, C.; Li, G. S.; Guan, X. F.; Luo, D.; Li, L. P. *Phys. Chem. Chem. Phys.* **2012**, *14*, 12368−12377.
(31) Xiao, J.; Chernova, N. A.; Whittingham, M. S. *Chem. Mater.* **2008**, *20*, 7454−7464.
(32) Wang, J.; Qiu, B.; Cao, H. L.; Xia, Y. G.; Liu, Z. P. *J. Power Sources* **2012**, *218*, 128−133.
(33) Li, J. G.; Wang, L.; Zhang, X.; He, X. M. *J. Power Sources* **2009**, *189*, 28−33.
(34) Johnson, C. S.; Li, N. C.; Lifief, C.; Vaughey, J. T.; Thackeray, M. M. *Chem. Mater.* **2008**, *20*, 6095−6106.
(35) Guo, X. J.; Li, Y. X.; Zheng, J. M.; Li, J.; Yang, Y. *J. Power Sources* **2008**, *184*, 414−419.
(36) Yu, S. H.; Yoon, T.; Mun, J. Y.; Park, S. J.; Oh, S. M.; Sung, Y. E. *J. Mater. Chem. A* **2013**, *1*, 2833−2839.